Discover Electrochemistry

RESEARCH Open Access

A gravitational electrochemical cell for *Operando* grazing incidence X-ray absorption spectroscopy experiments on industrial materials

Giuditta De Amicis[1], Anna Testolin[2], Francesco D'Acapito[3], Francesco Panico[5], Alberto Vertova[4,5], Paolo Ghigna[1,4*] and Alessandro Minguzzi[4,5,6]

*Correspondence:
Paolo Ghigna
paolo.ghigna@unipv.it

Full list of author information is available at the end of the article

Abstract

We present here a new design for an electrochemical cell that allows grazing incidence X-ray absorption spectroscopy (XAS) experiments to be performed. The idea is to have a laminar flow of electrolyte in front of the working electrode. In this way, the thickness of the electrolyte layer can be kept small enough to cope with the penetration depth of X-rays at the K-edges of 3d metals. The laminar flow is achieved by letting the electrolyte flow by gravity over a flat surface of the cell, where the working electrode is positioned. In this way, surface sensitivity can be achieved on bulk electrodes, as demonstrated by performing the water splitting reaction on nickel wires, which are the materials used in industrial conditions. The cell is easy to use and can be easily installed in an experimental hutch of an XAS beamline, the only requirement being to have enough space.

Keywords Raw nickel metallic's surface, *Operando* grazing incidence geometry, Laminar flux, New electrochemical cell, Oxygen evolution reaction

1 Introduction

Understanding the mechanism of chemical reactions taking place at the interface between a solid and another phase is crucial in many processes. For solid-gas interfaces, the phenomena involved range from gas sensing on semiconducting materials, to the uncountable catalytic reactions on different catalysts, such as metals, or oxides, or other compounds. In this case, the low density of the gas phase allows to match with the penetration depth of many spectroscopic probes, and performing *operando* experiments is reasonably easy.

Beside catalysis, reactions at a solid-liquid interface are of relevance to electrochemistry. In this case, a detailed mechanistic study of the relevant processes at the interface is often hindered by the fact that intrinsically surface sensitive techniques such as X-ray photoelectron spectroscopy (XPS), Auger electron spectroscopy (AES) or low

energy electron diffraction (LEED) are limited by the inelastic mean free path of electrons. Hard X-rays have the capability to deeply penetrate in an electrolytic solution, and X-ray absorption spectroscopy (XAS) has been widely used for mechanistic studies of electrode reactions. This is witnessed by specific reviews [1] and several research papers, including from our group and in many fields of electrochemistry [2–6], photochemistry [7] and photoelectrochemistry [2, 5–13]. However, per se, XAS is a bulk technique and access to surface phenomena is limited in this case and can be enhanced by instrumental approaches or by a correct sample design [14], for example by preparing the electrode materials in form of nanoparticles [3], that can be also characterized easily using the microcavity electrode technique, developed by some of us [15]. In this study, while ensuring an optimized surface-to-bulk ratio, the focus was on analyzing a surface metal, specifically nickel, used as a substrate for the preparation of DSA® electrodes. A DSA® electrode typically consists of a metal substrate, such as Ni for AWE (alkaline water electrolysis) conditions, coated with a layer of nanoparticles. However, the objective here was to isolate and study the contribution of the substrate surface alone to the reaction mechanism. This approach provides insights into the underlying role of the metallic substrate for the OER.

A way for making XAS surface sensitive is to collect the photoelectrons and all the other (secondary) electrons that are coming out from the sample: in this detection mode, which is called total electron yield (TEY), the probing depth is limited by the electron mean free path, which can be in the nanometer range, depending on the electron kinetic energy [16]. However, TEY is almost impossible to achieve in *operando* electrochemical conditions due to the presence of the electrolyte and of the applied potential, although recent efforts have been made in this respect in the soft X-ray regime [17].

As a matter of fact, XAS can be make intrinsically surface sensitive by detecting the intensity of the reflected beam from a flat surface. In this case, the technique is called ReflEXAFS, and surface sensitivity is achieved as below a critical angle the incoming beam is confined as an evanescent wave in a layer of sample which is of the order of few nanometers [18]. In this case, however, the total reflection condition requires: (i) an almost perfectly flat surface, and (ii) that the incident beam is perfectly collimated at the required incident angle. Although some recent efforts in this direction have been made with success [19], we here remark that these conditions may be difficult to achieve in real conditions, where the electrode surface is hardly flat, and the presence of concentrated electrolyte solution causes an isotropic background of scattered photons that impinge on the sample with random incidence angles. Finally, when the electrode is polarized at potentials where bubble formation occurs, acquiring XAS measurements becomes challenging. Under such conditions, the spectra obtained are often of low quality, lacking useful information.

In this paper, we present a simple electrochemical cell design for *operando* XAS experiments in grazing incidence, suitable for real working conditions and materials of industrial interest. The target reaction is the oxygen evolution reaction (OER), and both working and counter electrode are constructed using raw Ni wires as supplied by Industrie De Nora S.p.A. This is important as it can be a match for possible industrial conditions used in the production of green hydrogen.

In recent years, researchers have increasingly employed advanced cells for *operando* XAS studies [20]. Examples include three-dimensional printed multipurpose devices for spectro-photoelectrochemical characterization [2], an electrochemical cell setup for soft XAS studies [21], a versatile electrochemical cell for studying catalytic materials using X-ray diffraction and total scattering [22], air fuel cell for in-situ XANES experiments [23] and in-situ XAFS fuel cell [24]. Furthermore, considerable interest has focused on electrochemical cells with flow systems to better understand electrode-electrolyte interface behavior under *operando* condition [19, 25, 26].

In this work, we introduce a gravitational electrochemical cell, wherein the electrolyte solution flows over bulk nickel electrodes by gravity, ensuring a laminar flow that fully exploits surface sensitivity. This design maintains a thin electrolyte layer in front of the electrode, enabling grazing incidence experiments.

The key point here is the penetration depth of the X-rays: as the experiments were carried out at the Ni K-edge, as detailed below, we will describe the calculations at the pertinent energy (ca. 8333 eV). In water at 8333 eV, this can be estimated at about 1 mm. This means that if the X-ray beam travels a distance of 1 mm in the electrolyte solution before hitting the sample, it is attenuated by a factor of 1/e. Since the measurements are performed at grazing incidence, this distance is distributed in the direction of the incident beam, which means that the thickness of the electrolyte layer should be kept below $1\times\sin a$ mm, if a is the incidence angle. For $a\approx 2$ °, this is around 30 μm. Now, this thickness should cope with the electrochemistry, and this means that, if high current densities are desired, the electrolyte cannot stay still on the sample, otherwise it will be rapidly consumed. A laminar flow of electrolyte also avoids variations in the electrolyte thickness in front of the sample, that are detrimental for the XAS data acquisition, as it will shown in the following.

The capabilities of this device are demonstrated using metallic nickel electrodes as the anode in the water splitting reaction. Compared to state-of-the-art systems [60], this gravitational electrochemical cell facilitates OER studies under more challenging conditions, achieving higher potential values that are critical for understanding the reaction mechanism.

In this study, the focus was on analysing a metallic Ni surface, obtained by polishing a thick Ni wire. The choice of Nickel is due to its widely recognized used in several industrial applications, such as Alkaline Water Electrolysis (AWE), where Nickel is generally employed both as bare substrate or coated with catalytic layers (as for the so called DSA® electrodes).

Additionally, this design is compatible with a wide range of elements, including 3*d* transition metals for which the K-edge can be investigated, and heavier elements having the L_3-edge in the energy range between 5.5 and 15 keV (Ce to Fr), as the system has been designed to allow the use of a very thin electrolyte layer in front of the electrode. This feature makes it a powerful tool for the study of various materials, including industrially relevant electrode materials such as bulk metals and dimensionally stable anodes (DSA®) with low surface-to-bulk atomic ratios.

2 Experimental

2.1 Electrochemical cell design and construction

Electrochemical experiments were carried out using an Ivium Compactstat2.h potentiostat/galvanostat. No IR compensation was employed. The electrochemical cell was designed to ensure both suitable electrochemical performances and the capability of performing grazing incidence (GI) XAS experiments. The device, described in this work, is entirely made of epoxy resin (Epofix, Struers) with a specific ratio of 25:3 between epoxy resin and hardener. Technical specs of this resin indicate its resistance to acids, bases, acetone, alcohol. During testing and use for several hours in the present conditions, we never notices any sign of degradation, also when used for preparing microelectrodes [27]. The operational principle of the cell is based on letting a laminar layer of electrolyte to flow on the free surface of a bulk Ni electrode immersed in the resin, used as the anode in the water splitting reaction. A safe estimate of the affordable thickness of the laminar layer can be computed as follows: the absorption length of X-ray photons in water near the Ni K-edge (8333 eV) is 1.1 mm. This means that 1.1 mm of water reduces the beam intensity to a factor of $1/e$, still allowing a sizable photon flux on the sample. As we are interested in computing a safe estimate of the thickness of the film layer, using the absorption length is to be considered as legitimate. Assuming an incidence angle of 1 °, the thickness is of order of 1.1 mm × sin (1 °) = 20 μm. This means that with a flow thickness of 20 μm, a safe estimate of the lowest incidence angle is 1 °: we always used higher incidence angles (2 °) as detailed below. The target reaction is the oxygen evolution reaction, and both working and counter electrode are constructed using raw Ni wires as supplied by Industrie De Nora S.p.A. This is important as it can be a match for possible industrial conditions used in the production of green hydrogen.

Figure 1 illustrates the design of the mold for the gravitation electrochemical cell a, the physical mold made of PTFE b, and the epoxy resin casting process c. After a curing period of 12 h, the solidified cell was carefully removed from the stencil. Subsequently, a Kapton film was placed in front of the cell to maintain a thin and uniform electrolyte layer on the electrode surface d. This setup prevents the formation of water trickles and ensures uniform electrolyte flow across the entire surface.

The gravitational cell design, illustrating its key components, is sketched in Fig. 2.

To construct the cell, the Ni wire electrodes were positioned on a homemade Teflon mold, where the epoxy resin was cast. The working electrode (W.E.) is the key component where the main electrochemical reactions occur. The counter electrode (C.E.) allows the flow of current in the system and ensures the continuity of the electrochemical process. In this paper, both the W.E. and the C.E. are constructed using raw nickel wire. The surface area of both Ni wire electrodes, the working electrode (W.E.) and the counter electrode (C.E.), is 0.3 cm^2 (2 cm × 0.15 cm, length × height).

The distance between the WE and CE surfaces emerging from the resin was determined to be 6.7 mm. This value was dictated by the cell design and later verified by measuring it with a caliber.

The entire assembly was then let to cure for 12 h to become hard to be fixed in vertical position. Subsequently, the cell was removed from the mold, and polished, in the following order, with #800 #1000 and #4000 SiC paper and demineralized water. Finally, a DP-Nap cloth was used to finish polishing the electrodes. The polishing

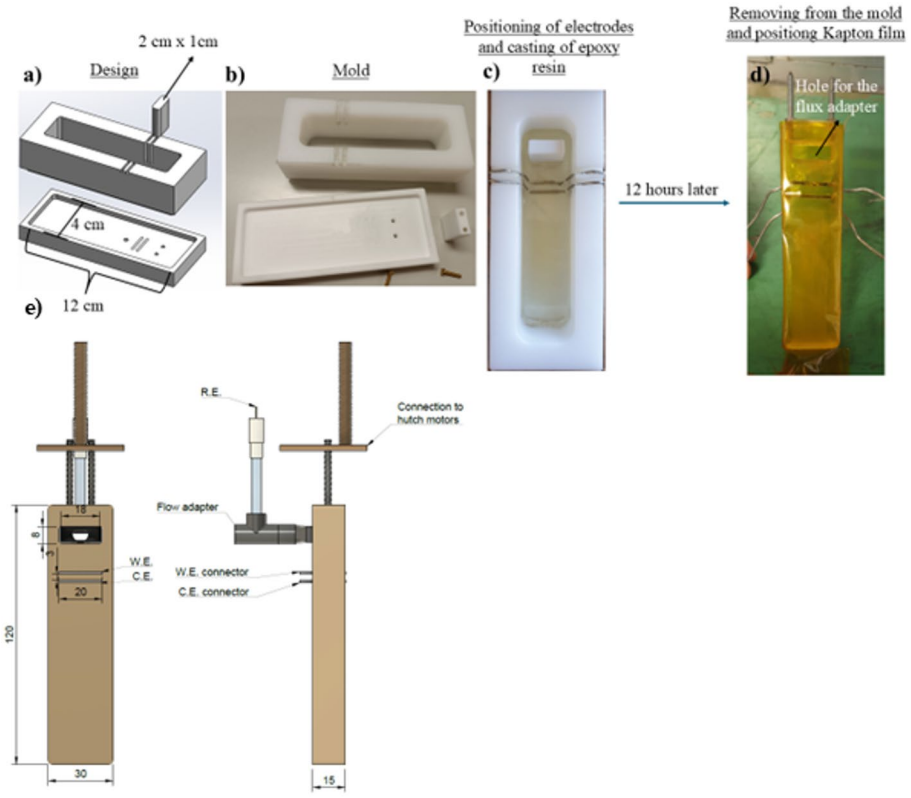

Fig. 1 **a** Design of the gravitational electrochemical cell mold. **b** PTFE mold. **c** Positioning of working and counter electrodes and epoxy resin casting process. **d** Removal of the cell from the stencil after 12 h and placement of a Kapton film in front of the cell to maintain a thin electrolyte layer on the electrode. **e** cell drawing with dimensions (in mm)

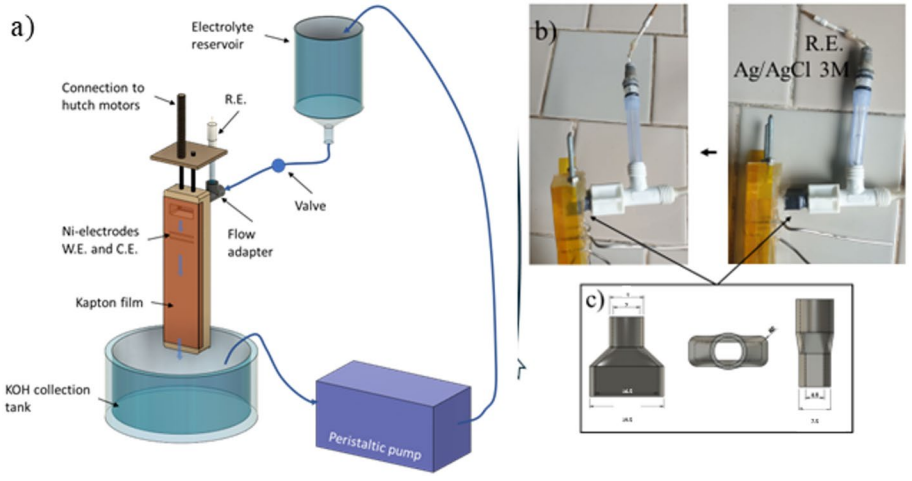

Fig. 2 **a** Representation of the gravitational cell design and set up. **b** Reference electrode positioned directly inside the flux tube. **c** Design of the laminar flux adapter to prevent electrolyte loss. It has a rectangular shape for the cell window and a circular shape for the electrolyte tubular flow. It was printed with a black Geeetech PLA (polylactic acid) filament on a *Anycubic i3 Mega* 3D printer. Distance between working electrode (W.E.) and counter electrode (C.E.) on the cell surface is 6.7 mm

was terminated when the exposed width of the electrodes, measured with a calibrate microscope, was found to be equal to the wire original diameter. The polishing process ensured a smooth surface to minimize possible interference with the laminar flux. Additionally, a polished and smooth surface is required for the acquisition of the XAS spectra with GI geometry. The reference electrode (RE) was an Ag/AgCl (in KCl 3 M solution), placed directly in the flux tube. Specifically, the RE was put in a tip with a solution of KNO_3 0.5 M as shown in Fig. 2 b. The electrolyte was KOH 0.1 M; the electrolyte is contained in a reservoir, which is placed higher than the cell, allowing the electrolyte to flow by gravity on the cell. The flow rate can be adjusted by a valve placed between the reservoir and the cell. A peristaltic pump was used to circulate the electrolyte at a flow rate of 50 mL min^{-1}. The peristaltic pump allows keeping the level of the electrolyte in the reservoir constant. This also helps in maintaining the laminar flow on the electrode constant. To facilitate the flux recycling, an adapter was fabricated with a rectangular shape for the cell window and a circular shape for the electrolyte tubular flow. The valve between the electrolyte reservoir and the cell can regulate the flux to be consistent with that imposed by the pump. The design of this component is shown in the box in Fig. 2c.

To avoid small variations over time in the thickness of the electrolyte layer in front of the electrode, which could cause significant disturbances in the spectra, a Kapton film was placed in front of the cell to maintain a thin layer of electrolyte on the electrode and to prevent the formation of water trickles. Between the Kapton and electrodes, spacers 20 μm thick were placed to ensure that the distance between the electrodes and Kapton foil was 20 μm. This was particularly important for effectively covering the entire electrode surface. Since Kapton is transparent to X-rays, it can be used for XAS acquisition. A representation of the entire set up in the hutch of the LISA (BM08) beamline at the ESRF synchrotron radiation facility is reported in Fig. 3. Prior to the XAS experiment, the formation of a uniform film of electrolyte on the electrode was checked by visual inspection; in addition, the continuity of the laminar flow on the cell was constantly monitored during the operando experiments by means of a closed-circuit television camera.

2.2 Grazing incidence data collection and analysis

Operando grazing incidence (GI) data at the Ni K-edge (E = 8333 eV) have been collected at the LISA BM08 beamline [28] operative at the European Synchrotron Radiation Facility (ESRF) on a dedicated experimental station [29].

Spectra of NiO and β-NiOOH were acquired in the transmission mode and used as standards for the Ni(II) and Ni(III) oxidation states, respectively [13]. For those measurements, an appropriate amount of sample (to give a unit jump in the absorption coefficient) was mixed with cellulose and pressed into a pellet. To provide a more accurate comparison with the working electrode, which was a nickel wire, measurements of a standard metallic Ni foil were also conducted.

All the experiments were performed using a 0.1 M potassium hydroxide solution (KOH, Sigma Aldrich) serving as supporting electrolyte in fluorescence mode. The X-Ray beam impinged on the sample in GI geometry with an incidence angle of ca. 2°, passing through the electrolyte solution. The beam size was 0.5×1 mm^2 (horizontal × vertical), which, in grazing incidence, gives a footprint on the sample of ca. 14×1 mm^2,

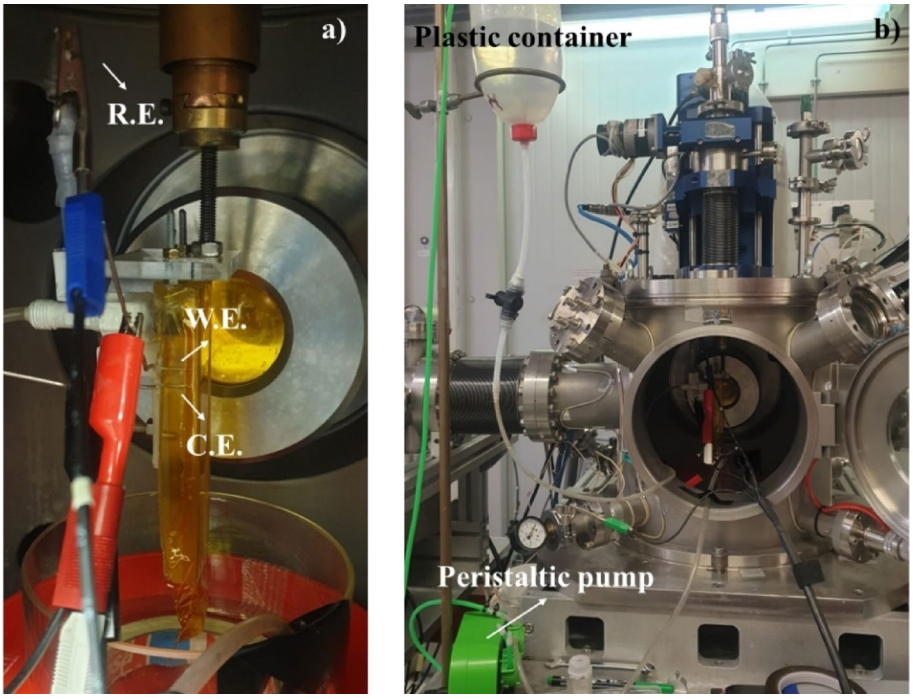

Fig. 3 Representation of the entire cell setup in the synchrotron hutch. In **a** the magnification of the electrochemical cell. In **b** the entire set up with the peristaltic pump, the tube for the flux, and the plastic container for electrolyte recirculation

which fully copes with electrode size of 20×1.5 mm^2 as detailed above. The fluorescence from the W.E. was collected by means of a 13 High Purity Germanium (HPGe) detector array. As each of the detector in the array observes the sample from a different angle, this allows for conducting some tests experiments in grazing emission (GE) mode, by using the detectors collecting the outcoming photons with the smallest receiving angle. The spectra were collected at the Ni K-edge from 300 eV before the edge to 12 k in the EXAFS region. A detailed description of the procedure for the cell alignment is provided in the SI. In addition, a plot of the reflectivity and fluorescence yield at 8400 eV as a function of the beam incidence angle is also shown in the SI (See Fig. S1). This last plot allows to justify the choice of the incidence angle of 2 °. Indeed, this is on the plateau of the fluorescence yield, but close to the maximum of reflectivity, allowing to safely assume that a significant part of the fluorescence originates from the surface of the sample. The repeatability of the experiments was checked by running the experiment in duplicate, and always obtaining the same results.

The oxidation state of nickel and the different oxides that are forming during the reaction, were evaluated by recording a series of XAS spectra at different fixed potential values, selected from previous electrochemical characterization. The selected values were: 0.43–1.08 V – 1.33–1.88 V – 1.98 V (vs. RHE). For each potential value, we acquired six spectra with a counting time of 3 s, to have a sensible signal to noise ratio and repeated the same sequence three times to check for data reproducibility, then we merged the spectra. For the X-Ray Absorption Near Edge Structure (XANES) analysis, the raw spectra were first background subtracted with a straight-line fitting to the pre-edge, and then normalized to unit absorption at 800 eV above the edge, where the EXAFS oscillations

are no longer visible, using the Athena [30–32]: the effectiveness of this normalization procedure is illustrated in Fig. S2.

3 Results and discussion

3.1 Electrochemical activity assessment

To study the Ni wire electrode and its electrochemical activity for the oxygen evolution reaction, cyclic voltammetry (CV) measurements were carried out in the potential range 0.9 V to 1.93 V (vs. reversible hydrogen electrode, RHE). The CV were executed in 0.1 M KOH, and were conducted before going to the ESRF. The set up used was the same as the one later utilized at the synchrotron for the XAS experiments.

All the measured currents were converted into current densities and all the potentials values were converted versus RHE. A typical cyclic voltammetry at 0.05 V s^{-1} is shown in Fig. 4.

Cathodic and anodic peaks are visible at about 1.3 V and 1.4 V (vs. RHE), respectively. These peaks can be attributed to the Ni(II)/Ni(III) redox couple. Both anodic and cathodic shoulders are visible during the oxidative and reductive sweeps [33]. Based on these results, we determined the potential values (indicated by arrows in Fig. 4) at which we conducted our experiments and acquired the XAS spectra.

It is worthwhile to underline the very high reachable current density obtainable with our cell: 21 mA/cm2 at 1.98 V vs. RHE, which allow to characterize the cell under more challenging working conditions, very relevant for industrial application.

The chrono-amperometry data recorded during the XAS spectra acquisition are shown in Fig. 5.

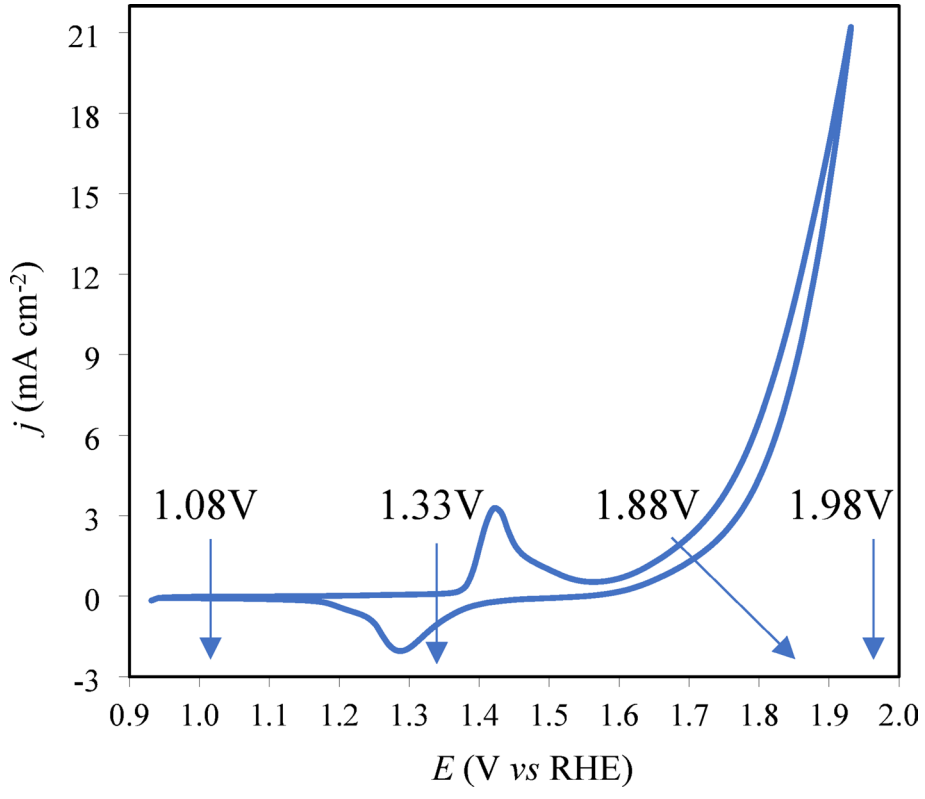

Fig. 4 Cyclic voltammetry of Ni wire done at 0.05 V s^{-1}

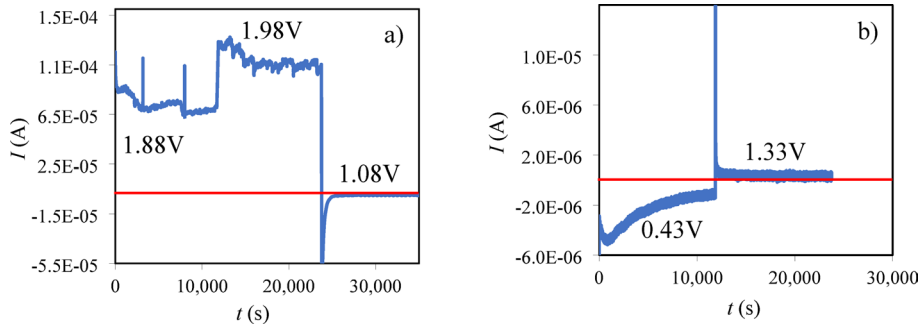

Fig. 5 Chrono-amperometry registered during the XAS spectra acquisition: in **a** the potential 1.88–1.98 V – 1.08 V versus RHE in **b** the potential 0.43–1.33 V versus RHE. In both **a** and **b** the current value of 0 A is highlighted in red

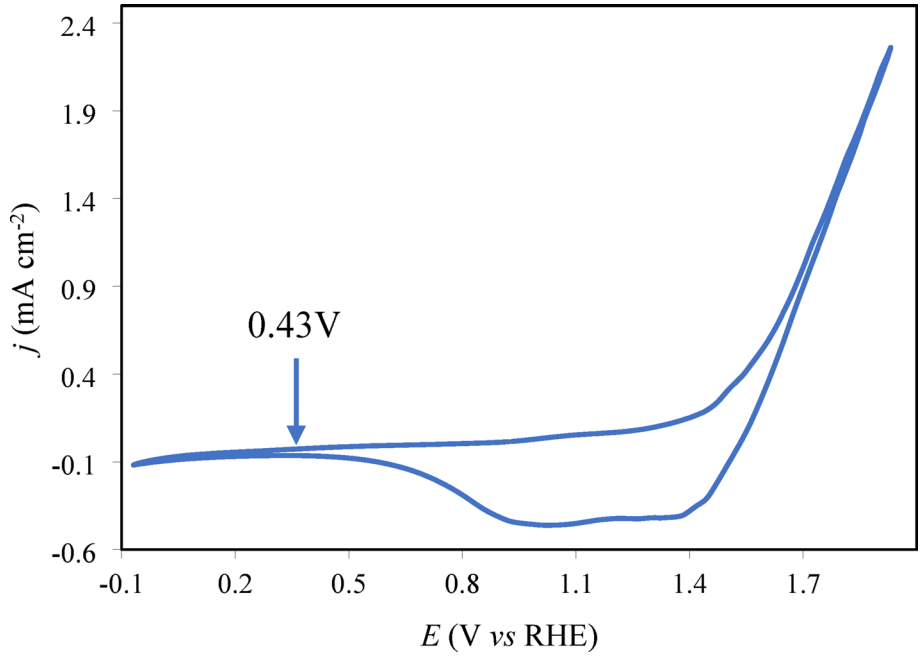

Fig. 6 Cyclic voltammetry of Ni wire at 0.1 V s^{-1} recorded after this sequence of XAS spectra at 1.88–1.98 V – 1.08 V

Overall, the registration is very stable, despite the length of each step, confirming the effectiveness of the cell in removing the formed bubbles. The chrono-amperometry at 0.43 V clearly shows a progressive current decay, that is likely due to the reduction of previously formed Ni-oxides. In fact, this measurement was conduct after acquiring the first three values (1.88–1.98 V – 1.08 V vs. RHE, Fig. 5a) and this choice was made after the observation of a significant reduction peak in cyclic voltammetry (Fig. 6). Moreover, we believe that the decreasing of current observed in Fig. 6 compared to Fig. 4 is due to the reduction of electrode active area as a consequence of Ni oxides layer formation after the strong anodic polarization at which the electrode was subjected. This also explains the lack of any anodic peak and the presence of, at least, two cathodic peak in Fig. 6. We decided to explore more cathodic potentials compared to the cyclic voltammetry reported in Fig. 4 because, after anodic polarization, a mixture of oxides with Ni in different oxidation states was formed. To understand when these oxides were fully reduced, we needed to go to – 0.1 V. Therefore, to verify if all species were effectively reduced

and no more Ni(III) was present, we decided to acquire XAS spectra at a more cathodic potential, specifically at 0.43 V.

During the XAS experiment (see below) we observed the formation of Ni(III) oxide at anodic potentials. Specifically, the formation began at 1.88 V and was confirmed at 1.98 V, where almost only Ni(III) was present. At 1.88 V, the spectra showed a mixture of Ni(II) and Ni(III). Going to more cathodic potentials, particularly to 1.08 V, Ni(III) disappeared, leaving only Ni(II). This observation was further confirmed by the CV (Fig. 6) recorded after this sequence of spectra in the potential range – 0.1 to 1.93 V (vs. RHE), where the oxidation peak of Ni(II) to Ni(III) was no longer visible due to the presence of Ni oxides layer on Ni surface formed during the XAS characterization. This also explains the two reduction peaks; they are due to the formation, during the anodic polarization, of a mixture of oxides with Ni in different oxidation states [34]. In addition, the reduction of all the Ni oxidized species required more cathodic potentials, particularly 0.43 V for the entire XAS acquisition time, where almost all nickel oxides are reduced to metallic Ni and Ni(II).

3.2 *Operando* grazing incidence experiments

From an experimental perspective, electrochemistry is first conducted to study the system and determine the potential of interest, at which the XAS spectra are subsequently acquired. The selected potentials include a cathodic potential of 1.08 V, where the current density is near zero; an intermediate potential of 1.33 V, positioned between the two peaks of Ni(II) and Ni(III); a potential of 1.88 V, where the oxygen evolution reaction (OER) begins; and a higher potential of 1.98 V, corresponding to high-pressure OER conditions. To confirm the complete reduction of all species and ensure the absence of Ni(III), additional XAS spectra were acquired at a more cathodic potential of 0.43 V.

First, we present the comparison between the spectra recorded at 1.33 V using GI geometry and grazing emission (GE) geometry (see the SI, Fig. S3 for schematic drawings of the two geometries): in this last case, the spectra were recorded by using perpendicular incidence and recording the fluorescence at low (ca. 5 °) emission angles, as described in the experimental section. The GE geometry spectrum is consistent with the presence of metallic Ni only, as it is evident by comparison with the spectra of the standard materials (compare the orange line in Fig. 7a with the blue line in Fig. 7b).

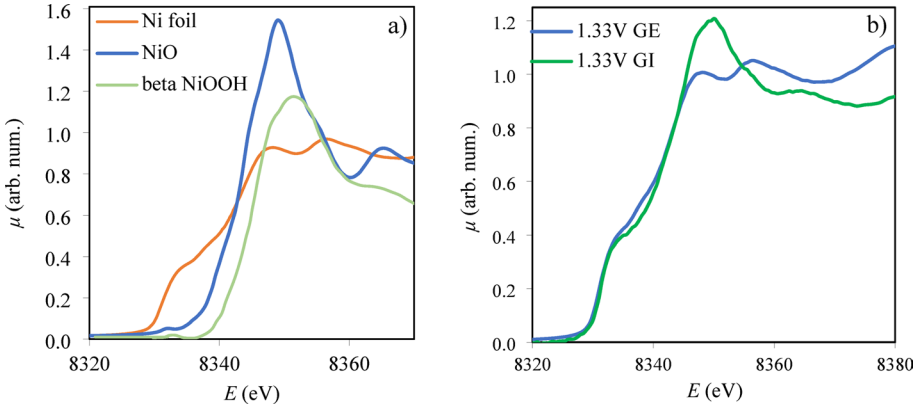

Fig. 7 Ni K-edge XANES in **a** the spectra of Ni foil, NiO and β-NiOOH are shown as reference of the edge position of Ni(0), Ni(II) and Ni(III). In **b** the comparison of the spectra recording at 1.33 V with GI and GE

GI was already employed in the study of several electrochemical systems [19, 35, 36]. In this work, the use of the gravitational cell design allows to obtain surface sensitivity with XAS on bulky materials. This is demonstrated by the fact that, in GI, a clear peak at ca. 8347 eV is detected, which is consistent with the presence of NiO (compare the blue line in Fig. 7a with the green line in Fig. 7b). This means that in GI we can probe, due to also the laminar flux without bubbles in front of the Ni, the oxidized surface Ni layer, which is not evident in GE geometry. This trend was consistent across all other spectra recorded at different potentials. We can also note that the spectra are free from artifacts due to variations in the electrolyte layer thickness, as evidenced by a direct comparison with the spectrum collected in non-laminar flow conditions, and reported in the SI (see Fig. S4).

The XANES spectra of the material under *operando* conditions recorded at different potentials with GI geometry are reported in Fig. 8.

We want here to emphasize that the sample is a raw Ni wire as supplied by the industry, without refining processing. This is because we preferred to study a sample whose structural and morphological features are close to those required for possible industrial applications, rather than being optimized for the XAS experiments.

All the spectra are consistent with the presence of some metallic Ni, which is evidenced by the shoulder at ca. 8333 eV. This contribution evidently originates from the Ni metal wire, which is in a very bulky state, and therefore this part of the spectrum is quite affected by self-absorption effects.

However, besides the metallic Ni, the presence of some oxidized Ni is clearly detected, as evidenced by the main edge peaks at ca. 8350 and 8354 eV, which, by comparison with Fig. 7a, are attributed to Ni(II) and Ni(III) oxidized species, respectively. At 1.3 V, i.e. where the CV shows that the oxygen evolution reaction (OER) is not started, the energy

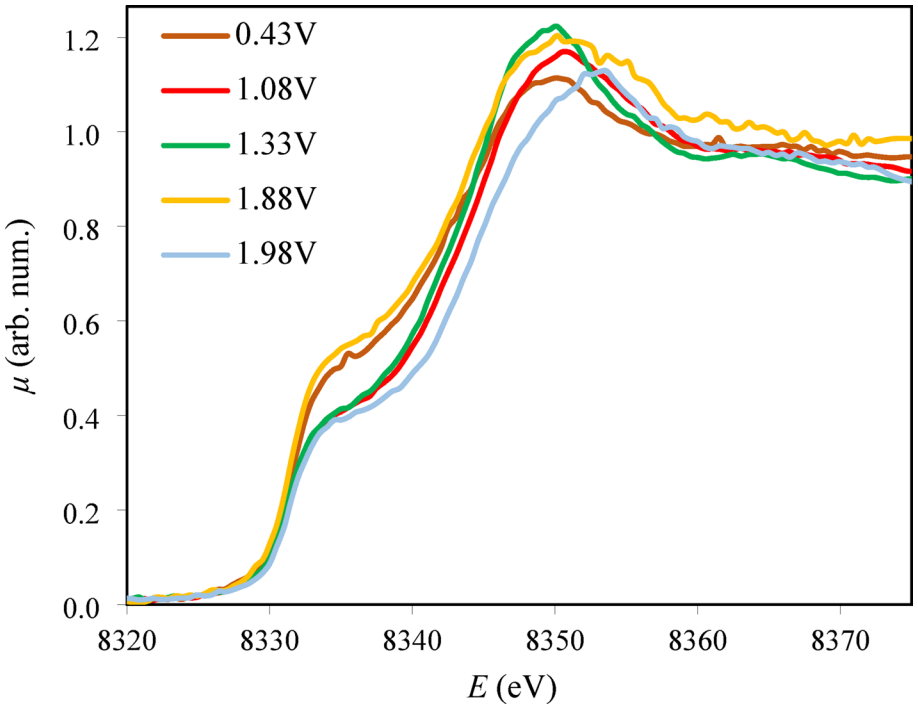

Fig. 8 Ni K-edge XANES of nickel metallic under *operando* conditions at different potentials with GI geometry

position of this peak is ca. 8350 eV, which is consistent with the presence of NiO or some other oxidic species of Ni(II). At 1.98 V, i.e. where the OER is taking place at the highest rate, Ni(III) formation is detected, as evidenced by the shifts towards higher energies of the main edge peak, in agreement with the spectra of the standards as shown in Fig. 7a. In addition, at 1.88 V, i.e. at a potential at which, according to the CV shown in Fig. 6, the OER is occurring at a lower rate, the presence of both Ni(II) and Ni(III) is detected, as indicated by the large and double-maximum peak. Finally, we note that in at 0.43 V, i.e. at the most cathodic potential, only Ni(II) is present.

The presence of metallic Ni in all the spectra may be attributed to the unavoidable presence of scattered photons by the electrolyte, which impinge on the sample at random angles, and therefore probe also the electrode bulk. In this respect, we can note that the X-ray beam from the LISA bending magnet source is well collimated, and the angular divergence of the beam is very small. The figures of the angular divergence are 0.003° and 0.05° in the vertical and horizontal directions, respectively. Therefore, we can exclude that the signal from bulk Ni is due to the angular dispersion of the impinging beam. Another source of the presence of metallic Ni in all the spectra can be the variation in the attenuation length of X-rays scanning across the edge. Looking at the data plotted in Fig. S5, one can see that the attenuation length in Ni shows a change in magnitude between 8330 and 8340 eV, passing from 900 to 100 nm. This shows that the data at low energy in the XANES are more sensitive to bulk metallic Ni.

In addition, the self-absorption and attenuation length variation effects involving the contribution from metallic Ni render a quantitative analysis difficult. For these reasons, we plotted the difference spectra, $\Delta\mu$, in Fig. 9, to reduce the metallic nickel contribution and enhancing the oxidic component.

Here the $\Delta\mu$ signal is obtained by subtracting from the spectra at each of the potential, the spectrum of the standard Ni foil used as reference, and shown in Fig. 7a. This method eliminates the metallic contribution and highlights the oxide contribution. For the sake of better comparison, in Fig. 9, we plotted also the same $\Delta\mu$ spectra obtained for NiO and NiOOH, that can be used as references for the Ni(II) and Ni(III) oxidation states, respectively. The $\Delta\mu$ spectra clearly evidence the main edge peak form the oxide: this becomes more pronounced at higher anodic potential values and shifts to ca. 8354 eV at potentials higher than 1.8 V, i.e. where the OER is taking place. We here discuss in detail the spectra at 1.33 V and 1.98 V, i.e. before and during the OER reaction. At 1.33 V, the $\Delta\mu$ spectrum shows a peak at 8350 eV, which is almost identical in spectral shape and position to that of the $\Delta\mu$ spectrum of NiO. We can therefore safely state that at this potential an oxidic layer is present, where Ni is in the Ni(II) oxidation state, and this holds also for lower potential values. At 1.98 V, the peak in the $\Delta\mu$ spectrum is shifted to ca. 8354 eV, and at this potential the $\Delta\mu$ is almost identical to that of NiOOH. Thus, at this potential, the oxidation state of Ni is steadily assigned to Ni(III). Finally, at 1.88 V, i.e. where the OER is evolving at lower rates, the very large shape of the peak in the $\Delta\mu$ spectrum is indicative of the presence of both Ni(II) and Ni(III), in agreement with the discussion above. As a final remark, we point out that the peak in the energy range between 8632 and 8735 eV ca. is directly due to electronic states, but is instead of structural origin. Indeed, this is the region where the EXAFS oscillations start. This peak does not shift in energy as a result of the potential changes, which indicates that

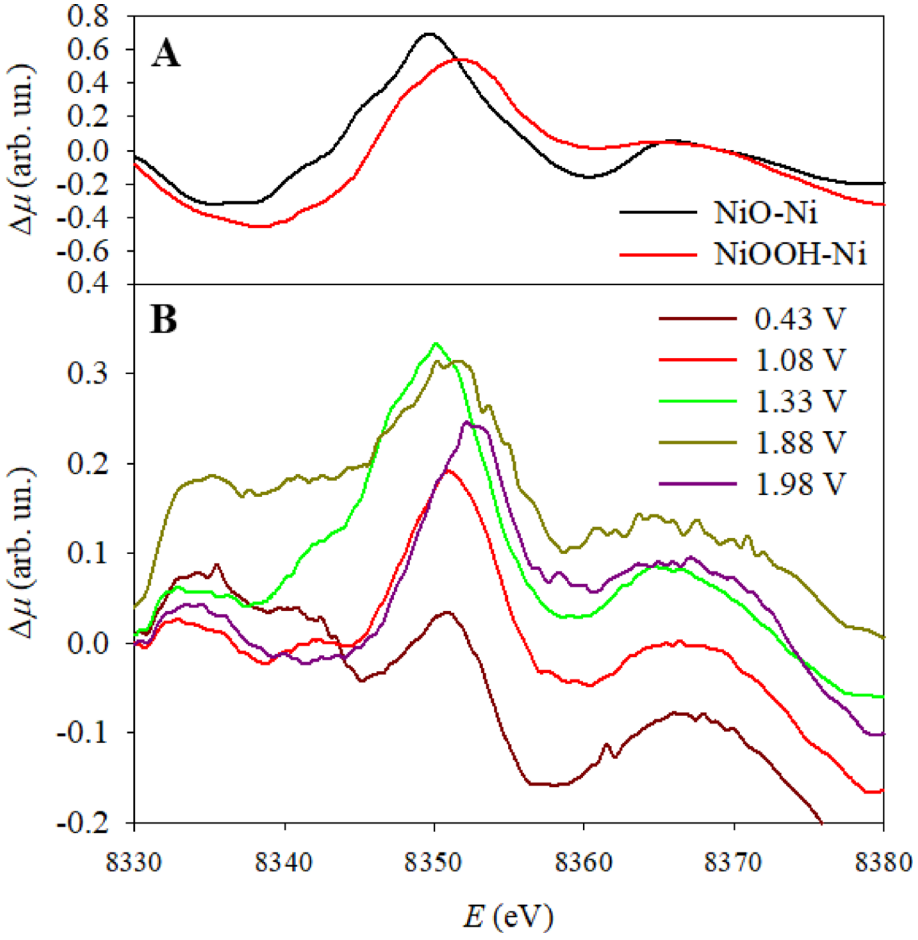

Fig. 9 **A**: $\Delta\mu$ spectra obtained by subtracting from the spectra of NiO and NiOOH the spectrum of metallic nickel. **B**: $\Delta\mu$ spectra obtained by subtracting at the spectra at each of the potential the standard spectrum of nickel metallic used as a reference

the Ni(III) centres are likely to reside on the very surface of the electrode, such that the structure of the NiO layer does not change.

4 Conclusions

This paper reports a preliminary communication about the feasibility of a gravitational spectro-electrochemical cell for operando experiments on materials of possible industrial interest. We have designed and built an electrochemical cell that allows a laminar flux of electrolytic solution to flow by gravity on metallic nickel electrode surface for *operando* XAS experiment in grazing incidence geometry. This setup enables the achievement of higher current densities and potential values compared to other similar studies. This improvement is attributed to the efficient removal of bubbles formed on the electrode surface, facilitated by the presence of a laminar flow induced by gravity. Thus, surface sensitivity is increased, permitting the study of a species that change with potentials at the electrode/solution interface and the detection of concomitant modifications in the electrode surface. This capability is useful for future studies of the mechanisms of this kind of reaction. Indeed, we succeeded in collecting spectra in *operando* conditions. This work, in addition to presenting the design and the construction of the electrochemical cell, highlights the study of a raw metal nickel surface during the oxygen evolution

reaction. We successfully recorded spectra in real conditions for a material whose structural and morphological features are close to those required for future industrial applications, rather than being optimized for XAS experiments.

We finally point out that the cell is reusable, and could be in principle be used with other materials: as a matter of fact, an improved design of this cell was recently and successfully employed by some of us in an experiment on the mechanisms of reduction of CO_2 on iron sulfides [37].

Supplementary Information

The online version contains supplementary material available at https://doi.org/10.1007/s44373-025-00071-5.

Supplementary Material 1

Acknowledgements

We are thankful to PON "Ricerca e Innovazione" 2014-2020, Azione IV.5 "Dottorati su tematiche green" DM1061-10.08.2021.G.D.A. gratefully acknowledge the Dipartimento di Chimica of the Università degli Studi di Milano for co-financing the project.Thanks are given to LISA, a project funded by the Consiglio Nazionale delle Richerche (project DFM.AD006.072). The experiment was the number A08-1/1114.AM acknowledge funding by: Funder: project funded under the National Recovery and Resilience Plan (NRRP), Mission 4 Component 2 Investment 1.3—Call for tender No. 341 of 15.03.2022 of Ministero dell'Universita e della Ricerca (MUR); funded by the European Union—NextGenerationEU. Award number: project code PE0000021, Concession Decree No. 1561 of 11.10.2022 adopted by Ministero dell'Universita e della Ricerca (MUR), CUP D43C22003090001, Project title "Network 4 Energy Sustainable Transition_NEST".AV and AM are grateful to Piano di Sostegno alla Ricerca 2023 (linea 2A) - Università degli Studi di MilanoProject funded under the National Recovery and Resilience Plan (NRRP), Mission 4 Component 2 Investment 1.3—Call for tender No. 1561 of 11.10.2022 of Ministero dell'Università e della Ricerca (MUR); funded by the European Union—NextGenerationEU Project code PE0000021, Concession Decree No. 1561 of 11.10.2022 adopted by Ministero dell'Università e della Ricerca (MUR), CUP D43C22003090001, project title "Network 4 Energy Sustainable Transition_NEST" through the project "Scalable innovative materials and devices for capture and valorisation of CO_2 to e-fuels" (eCO_2), CUP B53C22004060006. Jacopo Orsilli (LISA beamline) is kindly acknowledged for assistance duringthe XAS experiments.

Author contributions

G.DA. and P.G. wrote the main manuscript text and prepared the figures. A.V., P. G. and A. M. devised the experiment. G.DA., A.T. A.V., F.DA., F.P., A.M. and P.G. collected the experimental data. G.DA. and P.G. did the XAS data analysis. All Authors reviewed the manuscript.

Data availability

The datasets used and/or analysed during the current study are available from the corresponding author on reasonable request.

Declarations

Ethics approval and consent to participate

Not applicable.

Consent for publication

Not applicable.

Competing interests

The authors declare no competing interests.

Author details

[1]Dipartimento di Chimica, Università di Pavia, Viale Taramelli 16, 27100 Pavia, Italy
[2]Industrie De Nora S.p.A, Via Leonardo Bistolfi 35, 20134 Milan, Italy
[3]CNR-IOM-OGG LISA-CRG c/o ESRF, 71 Avenue des Martyrs, Grenoble, France
[4]Istituto Nazionale di Scienza e Tecnologia dei Materiali, via Giusti 9, Florence, Italy
[5]Dipartimento di Chimica, Università degli Studi di Milano, Via Golgi 19, 20133 Milan, Italy
[6]Dipartimento di Energia, Politecnico di Milano, Via Lambruschini, 4a, 20156 Milan, Italy

Received: 16 April 2025 / Accepted: 18 November 2025

Published online: 08 December 2025

References

1. Timoshenko J, Roldan Cuenya B. In situ/operando electrocatalyst characterization by X-ray absorption spectroscopy. Chem Rev. 2021;121(2):882–961. https://doi.org/10.1021/acs.chemrev.0c00396.

2. Baran T, Fracchia M, Vertova A, Achilli E, Naldoni A, Malara F, et al. Operando and time-resolved X-ray absorption spectroscopy for the study of photoelectrode architectures. Electrochim Acta. 2016;207:16–21. https://doi.org/10.1016/j.electacta.2016.04.153.
3. Minguzzi A, Locatelli C, Lugaresi O, Achilli E, Cappelletti G, Scavini M, et al. Easy accommodation of different oxidation states in iridium oxide nanoparticles with different hydration degree as water oxidation electrocatalysts. ACS Catal. 2015;5:5104–15. https://doi.org/10.1021/acscatal.5b01281.
4. Fracchia M, Visibile A, Ahlberg E, Vertova A, Minguzzi A, Ghigna P, et al. α- and γ-FeOOH: stability, reversibility, and nature of the active phase under hydrogen evolution. ACS Appl Energy Mater. 2018;1:1716–25. https://doi.org/10.1021/acsaem.8b00209.
5. Fracchia M, Cristino V, Vertova A, Rondinini S, Caramori S, Ghigna P, et al. Operando X-ray absorption spectroscopy of WO_3 photoanodes. Electrochim Acta. 2019;320:134561. https://doi.org/10.1016/j.electacta.2019.134561.
6. Achilli E, Minelli S, Casale I, He X, Agostini G, Spinolo G, et al. Determining the proton diffusion coefficient in highly hydrated iridium oxide films by energy dispersive X-ray absorption spectroscopy. Electrochim Acta. 2023;444:142017. https://doi.org/10.1016/j.electacta.2023.142017.
7. Achilli E, Vertova A, Visibile A, Locatelli C, Minguzzi A, Rondinini S, et al. Structure and stability of a copper(II) lactate complex in alkaline solution: a case study by energy-dispersive X-ray absorption spectroscopy. Inorg Chem. 2017;56:6982–9. https://doi.org/10.1021/acs.inorgchem.7b00553.
8. Altomare M, Qin S, Saveleva VA, Badura Z, Tomanec O, Mazare A, et al. Metastable Ni(I)-TiO_2-x photocatalysts: self-amplifying H_2 evolution from plain water without noble metal co-catalyst and sacrificial agent. J Am Chem Soc. 2023;145:26122–32. https://doi.org/10.1021/jacs.3c08199.
9. Baran T, Wojtyła S, Lenardi C, Vertova A, Ghigna P, Achilli E, et al. An efficient CuxO photocathode for hydrogen production at neutral pH: new insights from combined spectroscopy and electrochemistry. ACS Appl Mater Interfaces. 2016;8:21250–60. https://doi.org/10.1021/acsami.6b03345.
10. Braglia L, Fracchia M, Ghigna P, Minguzzi A, Meroni D, Edla R, et al. Understanding solid-gas reaction mechanisms by operando soft X-ray absorption spectroscopy at ambient pressure. J Phys Chem C. 2020;124:14202–12. https://doi.org/10.1021/acs.jpcc.0c02546.
11. Minguzzi A, Lugaresi O, Achilli E, Locatelli C, Vertova A, Ghigna P, et al. Observing the oxidation state turnover in heterogeneous iridium-based water oxidation catalysts. Chem Sci. 2014;5:3591–7. https://doi.org/10.1039/c4sc00975d.
12. Minguzzi A, Naldoni A, Lugaresi O, Achilli E, D'Acapito F, Malara F, et al. Observation of charge transfer cascades in α-Fe_2O_3/IrOx photoanodes by operando X-ray absorption spectroscopy. Phys Chem Chem Phys. 2017;19:5715–20. https://doi.org/10.1039/c6cp08053g.
13. Malara F, Fracchia M, Kmentová H, Psaro R, Vertova A, Oliveira De Souza D, et al. Direct observation of photoinduced higher oxidation states at a semiconductor/electrocatalyst junction. ACS Catal. 2020;10:10476–87. https://doi.org/10.1021/acscatal.0c02789.
14. Huang H, Russell AE. Approaches to achieve surface sensitivity in the in situ XAS of electrocatalysts. Curr Opin Electrochem. 2021;27:100681. https://doi.org/10.1016/j.coelec.2020.100681.
15. Vertova A, Barhdadi R, Cachet-Vivier C, Locatelli C, Minguzzi A, Nedelec JY, et al. Cavity microelectrodes for the voltammetric investigation of electrocatalysts: the electroreduction of volatile organic halides on micro-sized silver powders. J Appl Electrochem. 2008;38:965–71. https://doi.org/10.1007/s10800-008-9507-5.
16. Ruosi A, Raisch C, Verna A, Werner R, Davidson BA, Fujii J, et al. Electron sampling depth and saturation effects in perovskite films investigated by soft x-ray absorption spectroscopy. Phys Rev B. 2014;90:1–8. https://doi.org/10.1103/PhysRevB.90.125120.
17. Wang J, Hsu CS, Wu TS, Chan TS, Suen NT, Lee JF, et al. In situ X-ray spectroscopies beyond conventional X-ray absorption spectroscopy on deciphering dynamic configuration of electrocatalysts. Nat Commun. 2023. https://doi.org/10.1038/s41467-023-42370-8.
18. Costanzo T, Benzi F, Ghigna P, Pin S, Spinolo G, D'Acapito F. Studying the surface reaction between NiO and Al_2O_3 via total reflection EXAFS (ReflEXAFS). J Synchrotron Radiat. 2014;21:395–400. https://doi.org/10.1107/S1600577513031299.
19. Grespi A, Larsson A, Abbondanza G, Eidhagen J, Gajdek D, Manidi J, et al. Probing the electrode-liquid interface using operando total-reflection X-ray absorption spectroscopy. Surf Sci. 2024. https://doi.org/10.1016/j.susc.2024.122538.
20. Watanabe N, Morais J, Alves MCM. Design of an electrochemical cell for in situ XAS studies. J Electron Spectros Relat Phenomena. 2007;156–158:164–7. https://doi.org/10.1016/j.elspec.2006.12.021.
21. Jiang P, Chen JL, Borondics F, Glans PA, West MW, Chang CL, et al. In situ soft X-ray absorption spectroscopy investigation of electrochemical corrosion of copper in aqueous $NaHCO_3$ solution. Electrochem Commun. 2010;12:820–2. https://doi.org/10.1016/j.elecom.2010.03.042.
22. Frank S, Ceccato M, Jeppesen HS, Marks MJ, Nielsen MLN, Lu R, et al. The AUREX cell: a versatile operando electrochemical cell for studying catalytic materials using X-ray diffraction, total scattering and X-ray absorption spectroscopy under working conditions. J Appl Crystallogr. 2024;57:1489–502. https://doi.org/10.1107/S1600576724007817.
23. Viswanathan R, Hou G, Liu R, Bare SR, Modica F, Mickelson G, et al. In-situ XANES of carbon-supported Pt-Ru anode electrocatalyst for reformate-air polymer electrolyte fuel cells. J Phys Chem B. 2002;106:3458–65. https://doi.org/10.1021/jp013978 7.
24. Roth C, Martz N, Buhrmester T, Scherer J, Fuess H. In-situ XAFS fuel cell measurements of a carbon-supported Pt-Ru anode electrocatalyst in hydrogen and direct methanol operation. Phys Chem Chem Phys. 2002;4:3555–7. https://doi.org/10.1039/b204293b.
25. Paparoni F, Alizon G, Zitolo A, Rezvani SJ, Di Cicco A, Magnan H, et al. A novel electrochemical flow-cell for operando XAS investigations in X-ray opaque supports. Phys Chem Chem Phys. 2024;26:3897–906. https://doi.org/10.1039/d3cp04701f.
26. Erickson EM, Thorum MS, Vasić R, Marinković NS, Frenkel AI, Gewirth AA, et al. In situ electrochemical X-ray absorption spectroscopy of oxygen reduction electrocatalysis with high oxygen flux. J Am Chem Soc. 2012;134:197–200. https://doi.org/10.1021/ja210465x.
27. Zhao Z, Martino N, Tagliabue L, Minguzzi A, Vertova A. Facile preparation of robust and multipurpose microelectrodes based on injected epoxy resin. Electrochim Acta. 2023;437:141454. https://doi.org/10.1016/j.electacta.2022.141454.
28. D'Acapito F, Lepore GO, Puri A, Laloni A, La Manna F, Dettona E, et al. The LISA beamline at ESRF. J Synchrotron Radiat. 2019;26:551–8. https://doi.org/10.1107/S160057751801843X.

29. D'Acapito F, Davoli I, Ghigna P, Mobilio S. The ReflEXAFS station at the GILDA beamline (BM08) of ESRF. Synchrotron Radiat. 2003;10(3):260–4.
30. Ravel B, Newville M. ATHENA,ARTEMIS,HEPHAESTUS: data analysisfor X-ray absorption spectroscopy usingIFEFFIT. J Synchrotron Radiat. 2005;12:537–41. https://doi.org/10.1107/S0909049505012719.
31. Newville M. IFEFFIT: interactive XAFS analysis and FEFF fitting. J Synchrotron Radiat. 2001;8:322–4. https://doi.org/10.1107/S0909049500016964.
32. Maiwald MM, Dardenne K, Rothe J, Skerencak-Frech A, Panak PJ. Thermodynamics and structure of Neptunium(V) complexes with formate. Spectroscopic and theoretical study. Inorg Chem. 2020;59:6067–77. https://doi.org/10.1021/acs.inorgchem.0c00054.
33. Lyons MEG, Doyle RL, Godwin I, O'Brien M, Russell L. Hydrous nickel oxide: redox switching and the oxygen evolution reaction in aqueous alkaline solution. J Electrochem Soc. 2012;159:H932–44. https://doi.org/10.1149/2.078212jes.
34. Di Girolamo D, Piccinni M, Matteocci F, Marrani AG, Zanoni R, Dini D. Investigating the electrodeposition mechanism of anodically grown NiOOH films on transparent conductive oxides. Electrochim Acta. 2019;319:175–84. https://doi.org/10.1016/j.electacta.2019.06.170.
35. Winzely M, Clark AH, Balalta D, Chauhan P, Leidinger PM, Fikry M, et al. Monitoring the activation of a AuCu aerogel CO_2-reduction electrocatalyst via operando XAS. Langmuir. 2025;41:11026–36. https://doi.org/10.1021/acs.langmuir.5c00662.
36. Ren Y, Oyama J, Uchiyama T, Orikasa Y, Watanabe T, Yamamoto K, et al. State of the active site in La1−xSrxCoO3−δ under oxygen evolution reaction investigated by total-reflection fluorescence X-ray absorption spectroscopy. ACS Appl Energy Mater. 2022. https://doi.org/10.1021/acsaem.1c03327.
37. Panico F, Alessandri I, Ghigna P, Russell M, Minguzzi A. Vertova understanding hydrothermal vent electrochemical behaviour: a short-circuited fuel cell model. ChemRxiv. 2025. https://doi.org/10.26434/chemrxiv-2025-q54x9. This content is a preprint and has not been peer-reviewed.

Publisher's note